NEOPLASIA
www.neoplasia.com

Volume 18 Number 4 April 2016 pp. 253–263 253

Breast Cancer Heterogeneity Examined by High-Sensitivity Quantification of *PIK3CA*, *KRAS*, *HRAS*, and *BRAF* Mutations in Normal Breast and Ductal Carcinomas[1,2]

Meagan B. Myers*,[3], Malathi Banda*,[3], Karen L. McKim*, Yiying Wang*,[4], Michael J. Powell† and Barbara L. Parsons*

*US Food and Drug Administration, National Center for Toxicological Research, Division of Genetic and Molecular Toxicology, 3900 NCTR Rd., Jefferson, AR 72079; †DiaCarta, Inc., JOINN Innovation Park, 2600 Hilltop Drive, Richmond, CA 94806

Abstract

Mutant cancer subpopulations have the potential to derail durable patient responses to molecularly targeted cancer therapeutics, yet the prevalence and size of such subpopulations are largely unexplored. We employed the sensitive and quantitative Allele-specific Competitive Blocker PCR approach to characterize mutant cancer subpopulations in ductal carcinomas (DCs), examining five specific hotspot point mutations (*PIK3CA* H1047R, *KRAS* G12D, *KRAS* G12V, *HRAS* G12D, and *BRAF* V600E). As an approach to aid interpretation of the DC results, the mutations were also quantified in normal breast tissue. Overall, the mutations were prevalent in normal breast and DCs, with 9/9 DCs having measureable levels of at least three of the five mutations. *HRAS* G12D was significantly increased in DCs as compared to normal breast. The most frequent point mutation reported in DC by DNA sequencing, *PIK3CA* H1047R, was detected in all normal breast tissue and DC samples and was present at remarkably high levels (mutant fractions of 1.1×10^{-3} to 4.6×10^{-2}) in 4/10 normal breast samples. In normal breast tissue samples, *PIK3CA* mutation levels were positively correlated with age. However, the *PIK3CA* H1047R mutant fraction distributions for normal breast tissues and DCs were similar. The results suggest *PIK3CA* H1047R mutant cells have a selective advantage in breast, contribute to breast cancer susceptibility, and drive tumor progression during breast carcinogenesis, even when present as only a subpopulation of tumor cells.

Neoplasia (2016) 18, 253–263

Introduction

The advent of personalized medicine has created opportunities and challenges with respect to how the measurement and understanding of the underlying genetic lesions that cause cancer can be translated into improved health outcomes. Specific cancer mutations can inform cancer diagnosis and prognosis, and predict response to treatment and/or development of resistance to particular therapies [1–6]. Molecularly targeted therapies directed against the bulk of a cancer may create opportunities for the proliferation of minor subpopulations of cancer cells lacking the target, leading to cancer recurrence/progression and relapse. Knowledge regarding the prevalence and size of low frequency cancer subpopulations has the potential to inform the development of more efficacious and durable personalized cancer therapies and/or treatment strategies. Therefore, it is important to characterize cancer mutations using high-sensitivity methods, as a complement to the relatively low-sensitivity cancer genome characterizations that have been conducted [7–9].

Address all correspondence to: Barbara L. Parsons, US Food and Drug Administration, National Center for Toxicological Research, Division of Genetic and Molecular Toxicology, HFT-120, 3900 NCTR Road, Jefferson, AR 72079.
E-mail: barbara.parsons@fda.hhs.gov

[1] Conflict of interest statement: None declared.

[2] Author Contributions: BLP and MBM designed the study. YW, KLM, and BLP developed the ACB-PCR quantification of *PIK3CA* H1047R mutation. MBM developed the ACB-PCR quantification of *BRAF* V600E mutation. MB developed the ACB-PCR quantification of *HRAS* G12D. BLP, MBM, MB, and KLM collected the ACB-PCR data. MJP provided the QClamp measurements of *PIK3CA* H1047R mutation in normal breast DNA. BP and MBM conducted the statistical analyses of the data. All authors had input in writing the manuscript and approved the submitted version.

[3] Authors contributed equally to this work.

[4] Current Address: 102 Kanis Creek Lane, Little Rock, AR 72223.

Received 13 January 2016; Revised 22 February 2016; Accepted 1 March 2016

1476-5586
http://dx.doi.org/10.1016/j.neo.2016.03.002

Whole genome sequencing efforts have identified genes that drive breast cancer development when mutated. DNA sequencing detects mutations present at relatively high frequencies, although greater sensitivity can be achieved using non-standard methods [10,11]. *TP53* is the most frequently mutated gene in ductal carcinoma (DC, see Table 1), with *PIK3CA* the second most mutated gene. The *PIK3CA* gene encodes the p110α catalytic subunit of the class IA isoform of a lipid kinase, designated PI3-kinase (PI3K) [12]. According to the COSMIC or TCGA database, mutation of *PIK3CA* occurs in 22% (327/1551) or 24% of DCs, respectively [7,8,13]. The *PIK3CA* gene exhibits three hotspots for point mutation that encompass >90% of all reported *PIK3CA* mutations. These mutations are localized in the helical and kinase domains of the protein [14].

The *PIK3CA* H1047R mutation accounts for 56% of all *PIK3CA* mutations detected in DCs [7]. Other cancer-associated hotspot oncomutations have been reported in DCs, but no single base substitution mutation is as prevalent in DCs as the *PIK3CA* H1047R mutation (detected in 12% of DCs characterized by DNA sequencing) [7]. The *PIK3CA* H1047R mutation causes an overactivation of PI3K and enhances binding of PI3K to the cell membrane, which results in oncogenic transformation, increased cell proliferation, cell growth, survival, changes in gene expression, and altered invasion potential [14–17]. In advanced cancers, the *PIK3CA* H1047R mutation predicts increased partial response and progression-free survival in patients treated with PI3K/AKT/mTOR pathway inhibitors [16,18]. Conversely, the *PIK3CA* H1047R mutation is associated with clinical resistance to the EGFR-inhibitor, cetuximab [19].

RAS proteins play an important role in mammary signaling pathways, including the MAPK, PI3K and JAK-STAT pathways. These signaling pathways control important cellular functions, including cell proliferation, differentiation, migration and apoptosis. According to the COSMIC database [7], mutations in *KRAS* are present in only 2% (13/700) of DCs. Nevertheless, low frequency measurement of *KRAS* mutation in breast cancer is of interest, because minor *KRAS* mutant subpopulations (not detected by DNA sequencing) exist and have been shown to cause therapeutic resistance in other types of cancer [5,6]. Minor subpopulations of *KRAS* mutant cells (G12D and G12V), which exist in lung, thyroid, and colon cancers, have been quantified using Allele-specific Competitive Blocker PCR (ACB-PCR) [20–22]. Among PTCs, for example, 29% and 35% of cancers had mutant subpopulations of *KRAS* G12D and G12V, respectively, at levels greater than the upper 95% confidence interval of that present in normal thyroid, despite *KRAS* mutations being reported in only ~2% of PTCs by DNA sequencing [7]. DNA sequencing has detected *KRAS* G12D and G12V mutations in 3% and 4% of lung adenocarcinomas, respectively, but ACB-PCR demonstrated that 76% of the lung adenocarcinomas had a *KRAS* G12D or G12V mutant fractions (MFs) greater than the upper 95% confidence interval of that measured in normal lung [20]. Similar findings of prevalent *KRAS* mutant subpopulations in colonic adenomas and/or carcinomas have been obtained using ACB-PCR and other sensitive mutation detection methods [5,22]. In colorectal cancer (CRC) and non-small cell lung cancer (NSCLC), pre-existing *KRAS* mutant subpopulations can abrogate response to EGFR-targeted therapeutics (cetuximab, panitumimab, erlotinib, and gefitinib) [3,4].

HRAS mutations are prevalent in salivary gland, urinary tract, upper aerodigestive tract and cervical cancers (with *HRAS* mutant frequencies of 15%, 11%, 9%, and 9%, respectively) [23]. However, detection of *HRAS* mutations in breast cancers is rare (<1%) [23] and 0/508 DCs described in the COSMIC database carry *HRAS* mutation [7]. Somatic point mutations in *HRAS* occur most frequently at codons 12, 13 and 61 [7,23].

BRAF mutations are prevalent in malignant melanomas, PTCs, non-Hodgkin lymphomas, CRCs, and NSCLCs, but *BRAF* mutations have not been detected in DCs of the breast by DNA sequencing (0/522, see Table 1) [7]. Somatic point mutations in *BRAF* occur primarily in codon 600 of exon 15 and result in constitutive activation of the mitogen-activated protein kinase (MAPK) pathway. In fact, the *BRAF* V600E mutation (GTG to GAG) accounts for >95% of all reported *BRAF* mutations and has been associated with lack of response to therapies that target the EGFR [2].

Although *KRAS*, *HRAS* and *BRAF* mutations are rarely, if ever, detected in breast cancers by DNA sequencing, such mutations have been found in breast cancer cell lines [24], suggesting that breast cancers encompass minor *KRAS*, *HRAS* and *BRAF* mutant subpopulations that can be expanded in culture. Therefore, such mutations may be contributing to breast carcinogenesis in a manner that cannot be assessed by sequencing cancer DNA.

ACB-PCR is an allele-specific PCR amplification method that can quantify specific base substitution mutations when the mutation is present at a level of at least three mutant copies per 300,000 wild-type (WT) copies of a gene sequence (MFs of $\geq 10^{-5}$) in a given DNA sample. ACB-PCR has been used to quantify levels of cancer driver mutations in normal tissues and corresponding cancer samples in order to elucidate the potential for spontaneous mutations in normal tissues to drive tumor development, and evaluate the potential for specific mutant cancer subpopulations to impact acquired resistance to treatment, [20–22]. Here we apply this paradigm to normal breast tissues and DCs of the breast, examining cancer driver mutations that are either frequently detected in DCs or have been implicated in responses to personalized cancer treatments in other cancer types.

Table 1. Prevalence of gene mutations in ductal carcinomas of the breast.

Rank	Gene	Prevalence (%)
1	*TP53*	229/749 (31)
2	*PIK3CA*	321/1551 (21)
3	*GATA3*	10/52 (19)
4	*BRCA1*	13/90 (14)
5	*ARID1A*	9/78 (12)
6	*APC*	15/189 (8)
7	*CASC5*	3/45 (7)
8	*NUP98*	5/78 (6)
9	*AKAP9*	4/78 (5)
10	*PTEN*	13/256 (5)
11	*AKT1*	36/893 (4)
12	*KIT*	13/331 (4)
13	*NOTCH1*	5/113 (4)
14	*MYH9*	3/78 (4)
15	*MLL3*	3/78 (4)
16	*CDH1*	8/237 (3)
17	*BRCA2*	5/149 (3)
18	*KRAS*	13/700 (2)
19	*EGFR*	10/724 (1)
20	*ERBB2*	5/389 (1)
NR	*BRAF*	0/522 (0)
NR	*HRAS*	0/508 (0)

Data taken from the COSMIC database (www.cancer.sanger.ac.uk/cosmic), limited to ductal carcinomas. NR; not reported

Specifically, we used the sensitive and quantitative ACB-PCR approach to quantify five different hotspot cancer-driver mutations (*PIK3CA* H1047R, *KRAS* G12D, *KRAS* G12V, *HRAS* G12D, and *BRAF* V600E) in 10 normal breast and 9 DC samples.

Materials and Methods

Sample Collection

Procedures for the acquisition and analysis of anonymous human tissues were reviewed by the FDA Research Involving Human Subjects Committee (RIHSC, FWA 00006196). The intent of the study was to quantify mutations in normal breast and DCs. After obtaining the *PIK3CA* H1047R results, however, a parallel analysis of the same mutation in normal thyroid and papillary thyroid carcinomas (PTCs) was deemed necessary. These tissues were selected because PTCs carry *PIK3CA* mutation infrequently (2%) [7]. Ten fresh-frozen normal breast samples and 20 normal thyroid samples [21], collected at autopsy, were purchased from the National Disease Research Interchange (NDRI; Philadelphia, PA). Tissue donors died from causes unrelated to cancer or diseases affecting breast or thyroid. Nine fresh-frozen primary breast DCs and 20 fresh-frozen PTCs [21] were provided by the National Cancer Institute's Cooperative Human Tissue Network (CHTN). One PTC was purchased from NDRI. All cancer specimens were histologically evaluated by board certified pathologists, who confirmed the original diagnosis. One additional sample that was analyzed was a tumor margin. This sample was originally mislabeled as a DC, when in fact it was histologically characterized as breast fat with necrosis.

DNA Isolation

DNA from normal thyroid and PTCs was isolated as described previously [21]. Normal breast and breast DC tissue samples were frozen in liquid nitrogen, pulverized, and then DNA was isolated as described previously [21].

First-Round PCR

High-fidelity, first-round PCR amplicons encompassing human *PIK3CA* codon 1047, *KRAS* codon 12, *HRAS* codon 12, and *BRAF* codon 600 were performed using 1 μg of EcoRI-digested normal breast or DC genomic DNA as template. *PIK3CA* first-round PCR products, encompassing codon 1047, were generated using 1 μg of EcoRI-digested genomic DNA from normal thyroid and PTCs. For amplification of *KRAS*, *HRAS*, and *BRAF*, each 200 μl PCR reaction of contained: 10 mM KCl, 10 mM $(NH_4)_2SO_4$, 20 mM Tris–HCl (pH 8.75), 2 mM $MgSO_4$, 0.1% Triton X-100, 0.1 mg/ml bovine serum albumin, 0.2 mM dNTPs, and 10 units of cloned *PfuUltra* Hotstart DNA Polymerase (Agilent Technologies, Santa Clara, CA). The conditions used for *PIK3CA* first-round PCR were identical, except that 12.5 units of cloned *PfuUltra* Hotstart DNA Polymerase were used. All PCR experiments were carried out using DNA Engine or DNA Engine Tetrad thermocyclers (Bio-Rad, Hercules, CA). Primer sequences and thermocycler reaction conditions for each target are given in Supplementary Materials (Table S1). Following preparative agarose gel electrophoresis, *PIK3CA, KRAS*, and *BRAF* PCR products were isolated using a Geneclean Spin Kit (MP Biomedicals, Solon, OH), and recovered in TE buffer (5 mM Tris, 0.5 mM EDTA, pH 7.5). *HRAS* PCR products were purified by ion-pair reverse phase chromatography using a WAVE Nucleic Acid Fragment Analysis System (Transgenomics Inc, Omaha, NE). PCR products were evaporated to dryness and resuspended in TE buffer. All PCR products were frozen as multiple single-use aliquots. The DNA concentrations of aliquots were established by repeated measurement using an Epoch Spectrophotometer (BioTek, Winooski, VT). The final DNA concentration of each amplicon (*PIK3CA*, *KRAS*, *HRAS*, and *BRAF*) was calculated from three determinations that varied by ≤10% from the group mean.

ACB-PCR

ACB-PCR is an allele-specific amplification method that: 1) relies upon parallel a set of mutant fraction (MF) standards analyzed in parallel with first-round PCR products generated from unknown samples (comparing equal numbers of molecules), and 2) can be used to selectively amplify and quantify a mutant allele in a 100,000-fold excess of WT allele. *KRAS* G12D (codon 12 GAT) and G12V (codon 12 GTT) mutant and *KRAS* WT (codon 12 GGT) standards were prepared by digestion of cloned mutant or WT plasmid DNAs with AflII and AvaII and isolation of a DNA segment identical in sequence composition to the first-round PCR product prepared from isolated breast DNA samples. Mutant *PIK3CA* H1047R (codon 1047 CGT), *HRAS* G12D (codon 12 GAC), and *BRAF* V600E (codon 600 GAG) and WT standards (*PIK3CA* codon 1047 CAT, *HRAS* codon 12 GGC, and *BRAF* codon 600 GTG) were prepared by PCR amplification of cloned mutant or WT plasmid DNAs, using the same primers and conditions used for amplification of the target sequence from genomic DNAs (see Table S1). Purification of *PIK3CA* and *BRAF* WT, mutant, and unknown PCR products was performed using preparative agarose gel electrophoresis as described above. Purification of *HRAS* mutant, WT and unknown PCR products was accomplished by ion-pair reverse phase chromatography using a Transgenomic WAVE Nucleic Acid Fragment Analysis System.

For each ACB-PCR assay, purified *PIK3CA, KRAS*, *HRAS*, or *BRAF* mutant and WT reference DNAs were mixed to generate standards with MFs of 10^{-1}, 10^{-2}, 10^{-3}, 10^{-4}, 10^{-5}, and 0 (containing only the WT sequence), at a concentration of 5×10^7 copies/μl for the *PIK3CA, KRAS*, and *BRAF* standards, and 10^8 copies/μl for the *HRAS* standards. Each ACB-PCR reaction incorporated 10 μl of each DNA mixture, for a total of 5×10^8 copies per reaction for *PIK3CA*, *KRAS*, and *BRAF* assays, and 10^9 copies per reaction for *HRAS*. Each MF standard was analyzed in duplicate, along with a no-DNA control. The ACB-PCR was performed in a 96-well PCR plate (Thermo Fisher Scientific, Waltham, MA). The ACB-PCR primer sequences and thermocycler reaction conditions used for each target are given in Supplementary Material (Table S2).

QClamp XNA-PCR

QClamp XNA-PCR is a real-time PCR technology that utilizes a sequence specific oligonucleotide blocker that has a modified backbone chemistry. The use of a modified backbone increases the binding affinity and hence the melting temperature (Tm) of the blocking oligomer which leads to more efficient clamping of WT alleles [25]. The binding of sequence specific XNA oligomers is independent of salt concentration as the backbone has no ionic charge. The XNA-PCR reaction conditions used in the quantification of the *PIK3CA* H1047R mutation were 95°C for 300 seconds, followed by 40 cycles of 95°C for 20 seconds, 70°C for 20 seconds, and 60°C for 60 seconds.

Vertical Polyacrylamide gel Electrophoresis, Image Analysis, and Data Collection

Equal volumes of ACB-PCR products were analyzed on non-denaturing 8% polyacrylamide gels, loading 10 μl of *KRAS* and *BRAF* ACB-PCR products or 15 μl of the *PIK3CA and HRAS* ACB-PCR products. The fluorescent ACB-PCR products were visualized using a PharosFX Molecular Imager with an external blue laser (Bio-Rad). Pixel intensities of the correct-sized bands were quantified using Quantity One software and a locally-averaged background correction (Bio-Rad). Although duplicate 10^{-1} to 10^{-5} MF standards were included in each experiment, the set of standards that gave the best quantification across the observable range of MFs for an entire set of unknown samples was used to construct each standard curve [10^{-5} to 10^{-1} for *PIK3CA* and *BRAF*, 10^{-5} to 10^{-3} for *KRAS* and *HRAS*]. For *PIK3CA* and *KRAS*, log-log plots relating MF to fluorescence (in pixels) were constructed and fit with a power function. For *BRAF*, log-linear plots relating MF to fluorescence were constructed and fit with a logarithmic function. For *HRAS*, linear-linear plots relating MF to fluorescence were constructed and fit with a linear function. Using the function of the standard curve and the pixel intensities of the ACB-PCR products for each mutation, the MF of each mutation within each unknown sample was calculated.

Statistical Analyses

For each sample/target, MF was calculated as the arithmetic average of three independent MF measurements. Calculated MFs less than the smallest ACB-PCR MF standard employed (MF of 10^{-5}) are reported as non-detects (ND) in Table 2. The average MF measurement for each sample was $\log_{10}$-transformed. For each mutational target, the geometric mean MF was calculated as the average $\log_{10}$-transformed MFs measured in a particular tissue type (breast, thyroid, DC, or PTC). Log_{10}-transformed data were used for statistical analyses. Because not all log-transformed data were normally distributed, non-parametric analyses (Mann–Whitney rank sum test or Fisher's exact test) were employed to identify significant differences between MFs in normal tissue and cancer tissue. The Mann–Whitney rank sum test was used when a quantitative ranking of MFs was possible (breast *PIK3CA* H1047R, *KRAS* G12D, and *HRAS* G12D). Fisher's exact test was used when datasets contained multiple samples below the levels of accurate ACB-PCR quantification (10^{-5}), and compared the numbers of samples with MFs $>10^{-5}$ and $<10^{-5}$ in normal and cancer tissue (breast *KRAS* G12D, breast *BRAF* V600E, and thyroid *PIK3CA* H1047R). Pearson correlation coefficients, between donor age and MF, were determined using normally-distributed, log-transformed data and considering only samples with measureable MFs ($>10^{-5}$). Two-tailed p-values of less than 0.05 were considered significant. All statistical analyses were performed using GraphPad Prism 5 Software (GraphPad Software, Inc., La Jolla, CA).

Results

To elucidate the role of hotspot cancer driver mutations in breast carcinogenesis, quantitative profiles of several such mutations were generated for normal breast and DCs using ACB-PCR. The mutational targets included: 1) the most frequently reported point mutation in DCs (*PIK3CA* H1047R), 2) mutations that have been reported rarely in DCs, but are present as subpopulations in other cancer types (*KRAS* G12D and *KRAS* G12V), and 3) mutations that have not been observed in DCs (*HRAS* G12D and *BRAF* V600E). The levels of these mutations were measured in ten normal breast tissues, nine DCs and one fat sample with necrosis (associated with a DC). The *PIK3CA* H1047R, *KRAS* G12D, *KRAS* G12V, *HRAS* G12D, and *BRAF* V600E MF measurements of the twenty samples generated a dataset of 299 individual ACB-PCR measurements. Each unknown was quantified in three independent experiments (except sample #2, with only 2 *KRAS* G12D measurements). The average coefficient of variation for the triplicate *PIK3CA* H1047R, *KRAS* G12D, *KRAS* G12V, *HRAS* G12D and *BRAF* V600E MF measurements were 0.83, 0.69, 0.63, 0.70, and 0.27, respectively.

Table 2. Individual MF measurements of five hotspot cancer driver mutations in normal breast and ductal carcinomas.

	ID	Age/Race	*PIK3CA* H1047R MF	*KRAS* G12D MF	*KRAS* G12V MF	*HRAS* G12D MF	*BRAF* V600E MF
Normal Breast	1	83/C	4.59×10^{-2}	4.66×10^{-5}	5.66×10^{-5}	1.43×10^{-4}	ND
	2	87/C	1.07×10^{-2}	7.88×10^{-5}	1.63×10^{-5}	1.17×10^{-4}	ND
	3	60/C	1.93×10^{-2}	8.27×10^{-5}	7.40×10^{-6}	1.10×10^{-4}	ND
	4	63/C	1.06×10^{-2}	1.73×10^{-4}	4.06×10^{-5}	8.40×10^{-5}	ND
	5	68/C	1.95×10^{-4}	1.29×10^{-4}	1.98×10^{-5}	2.91×10^{-6}	ND
	6	67/C	1.03×10^{-3}	9.78×10^{-5}	1.25×10^{-5}	2.23×10^{-4}	ND
	7	49/C	1.25×10^{-5}	1.45×10^{-4}	1.01×10^{-5}	5.28×10^{-5}	ND
	8	43/AA	4.14×10^{-5}	2.50×10^{-5}	ND	1.78×10^{-4}	ND
	9	29/AA	4.76×10^{-5}	2.98×10^{-5}	ND	3.37×10^{-5}	ND
	10	23/AA	1.69×10^{-4}	4.75×10^{-5}	ND	8.15×10^{-5}	1.74×10^{-4}
		***Geomean**	$\mathbf{7.80 \times 10^{-4}}$	$\mathbf{7.13 \times 10^{-5}}$	$\mathbf{1.23 \times 10^{-5}}$	$\mathbf{6.94 \times 10^{-5}}$	$\mathbf{2.02 \times 10^{-6}}$
Ductal Carcinomas	1	40/AA	2.97×10^{-2}	2.87×10^{-5}	3.81×10^{-5}	3.16×10^{-4}	ND
	2	45/AsA	1.57×10^{-5}	2.21×10^{-5}	ND	2.71×10^{-4}	ND
	3	47/C	4.37×10^{-2}	4.86×10^{-5}	ND	3.58×10^{-4}	ND
	4	50/C	1.24×10^{-2}	4.81×10^{-5}	ND	3.83×10^{-4}	ND
	5	60/C	1.84×4^{-4}	3.54×10^{-5}	1.13×10^{-5}	1.38×10^{-4}	ND
	6	42/C	9.26×10^{-5}	2.16×10^{-4}	1.33×10^{-5}	1.93×10^{-4}	ND
	7	60/C	1.18×10^{-2}	3.55×10^{-5}	2.58×10^{-5}	1.90×10^{-4}	ND
	8	62/C	3.86×10^{-4}	8.99×10^{-5}	2.31×10^{-5}	1.54×10^{-4}	2.28×10^{-4}
	9	38/C	7.24×10^{-5}	8.63×10^{-5}	1.70×10^{-5}	1.77×10^{-4}	3.27×10^{-4}
		***Geomean**	$\mathbf{1.04 \times 10^{-3}}$	$\mathbf{5.27 \times 10^{-5}}$	$\mathbf{1.37 \times 10^{-5}}$	$\mathbf{2.27 \times 10^{-4}}$	$\mathbf{6.49 \times 10^{-6}}$

*Group geomeans were estimated using individual MFs calculated from ACB-PCR pixel intensities and standard curves, even when measured MFs were below 10^{-5} (noted as non-detects, ND).

Replicate examples of the ACB-PCR output for each mutational target are provided in Supplementary Material (Figure S1). Following ACB-PCR, MF quantification was achieved by interpolation of fluorescent intensities of unknown samples with that of a standard curve constructed using samples with defined ratios of mutant:WT alleles (*i.e.*, duplicate 10^{-1}, 10^{-2}, 10^{-3}, 10^{-4}, 10^{-5} and 0 standards). A representative example of a standard curve used for each mutational target is shown in Supplementary Material (Figure S2). For the *PIK3CA* H1047R MF measurements, the average coefficient of determination (r^2) for the standard curves was 0.9459 (range 0.9346 to 0.9586). For the *KRAS* GAT MF measurements, the average r^2 for the standard curves was 0.9936 (range 0.9876 to 0.9965). For the *KRAS* GTT MF measurements, the average r^2 for the standard curves was 0.9945 (range 0.9905 to 0.9973). For the *HRAS* G12D MF measurements, the average r^2 for the standard curves was 0.9809 (range 0.967 to 0.9914). For the *BRAF* V600E MF measurements, the average r^2 for the standard curves was 0.9939 (range 0.9869 to 0.9953).

MF Measurements in Normal Breast

The normal breast samples were derived from ten women, 23–87 years of age (57.20 ± 21.19, mean years of age ± SD), which included seven Caucasian and three African American women. The average ACB-PCR MF measurement for each target mutation in each normal breast sample is given in Table 2. For *PIK3CA* H1047R and *KRAS* G12D, 10/10 (100%) of normal breast samples had measureable levels of mutation (*i.e.*, $>10^{-5}$, the lowest standard employed, see Figure 1, *A* and *B*). For *HRAS* G12D, *KRAS* G12V, and *BRAF* V600E, 9/10 (90%), 6/10 (60%), and 1/10 (10%) of normal breast samples had measureable levels of mutation (see Figure 1*C*, 1D, and 1E), respectively. The *PIK3CA* H1047R, *KRAS* G12D, *KRAS* G12V, *HRAS* G12D, and *BRAF* V600E geometric mean MFs for normal breast were 7.80×10^{-4}, 7.13×10^{-5}, 1.23×10^{-5}, 6.94×10^{-5}, and 2.02×10^{-6}, respectively (Table 2). A linear regression analysis, describing the relationship between age and *PIK3CA* H1047R MF in normal breast, is shown in Figure 2. There is a positive correlation between tissue donor age and *PIK3CA* H1047R MF (Pearson $r = 0.7130$, $P = .0206$). No significant correlation was observed between the age of the tissue donor and *KRAS* G12D, *KRAS* G12V, or *HRAS* G12D MF in normal breast tissue (there were too few normal breast samples with *BRAF* V600E MFs $>10^{-5}$ to perform a correlation analysis).

Given the remarkably high levels of *PIK3CA* H1047R mutation detected in 4/10 normal breast tissue samples, a second sensitive mutation detection method was employed to confirm the ACB-PCR results. The QClamp™ Gene Mutation Test (DiaCarta, Inc., Richmond, CA) is an allele-specific PCR method that employs a xenonucleic acid "clamp" to suppress amplification of WT sequence. The QClamp method can detect mutations when present in a DNA samples at a level of 0.05% (MF = 5×10^{-4}, see Supplementary Material, Table S3 and Figure S3). This is consistent with the observation that the QClamp™ method did not detect *PIK3CA* H1047R mutation in samples that had ACB-PCR MFs less than 5×10^{-4} (see the comparison on MF measurements obtained using QClamp™ and ACB-PCR, provided in Supplementary Material, Table S4). The QClamp™ and *PIK3CA* MF measurements were

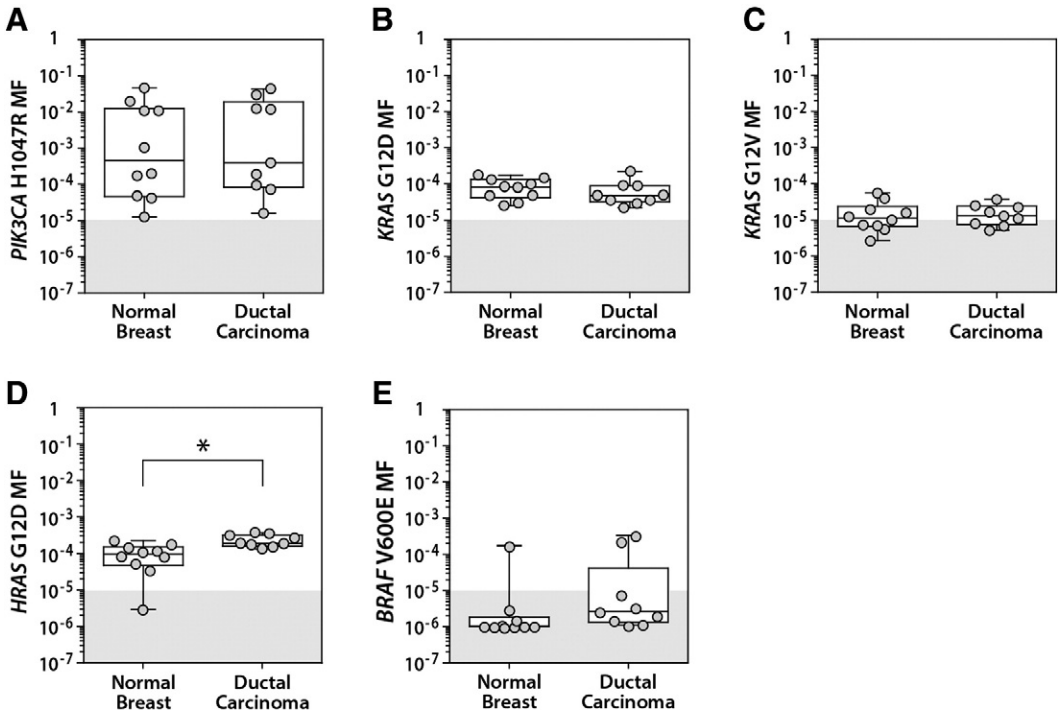

Figure 1. Frequency distributions of individual MF measurements in normal breast and DCs for *PIK3CA* (A), *KRAS* G12D (B), *KRAS* G12V (C), *HRAS* G12D (D), and *BRAF* V600E (E). Individual measurements are plotted along with box and whisker plots indicating the 5th, 25th, 50th, 75th, and 95th percentiles for each population distribution of MF measurements. Measurements in the shaded areas ($<10^{-5}$) are below the limit of accurate ACB-PCR quantification. The * indicates a significant difference in *HRAS* G12D MFs in DCs as compared to normal breast (two-tailed, Mann–Whitney rank sum test; $P = .0033$).

Figure 2. Linear regression between normal breast tissue donor age and *PIK3CA* H1047R MF. Dashed lines describe the 95% confidence interval.

generally in good agreement for normal breast samples with *PIK3CA* H1047R MFs greater than 10^{-3}. Regarding the four samples that had measureable mutation using both methods, the ACB-PCR measurements were 2.2- to 3.3-fold greater than the corresponding QClamp™ measurements (see Supplementary Material, Table S4). The ACB-PCR assay may be overestimating the *PIK3CA* MF somewhat, given that the ACB-PCR standard curves used to calculate *PIK3CA* H1047R MF covered a range of five orders of magnitude and had lower coefficients of determination than the QClamp™ standard curve (r^2 = 0.9459, on average, for three replicate ACB-PCR assays vs r^2 = 0.9983 for the QClamp™ assay). Nevertheless, the QClamp™ analysis confirmed that there are remarkably high levels of *PIK3CA* mutation in 4/10 (40%) of the normal breast tissue samples (QClamp™ MF levels between 3.7×10^{-3} and 2.1×10^{-2}). These measurements suggest that 4/10 normal breast tissue samples carry one PIK3CA H1047R mutant cell per every 24 to 135 PIK3CA WT cells.

MF Measurements in DCs

DCs were derived from nine women, 38–65 years in age (49.33 ± 9.23, mean years in age ± SD), including eight Caucasians, one African American, and one Asian American. The patient and tumor characteristics for the nine DCs are given in Supplementary Material (see Table S5). The average ACB-PCR measurement for each mutation in each DC sample is given in Table 2. All nine DCs had measurable levels ($\geq 10^{-5}$) of *PIK3CA* H1047R, *KRAS* G12D, and *HRAS* G12D mutations (see Figure 1*A*, *B*, and *D*). For *KRAS* G12V and *BRAF* V600E, 6/9 and 2/9 DCs had MFs greater than the lowest standard employed (10^{-5}, see Figure 1, *C* and *E*). The *PIK3CA* H1047R, *KRAS* G12D, *KRAS* G12V, *HRAS* G12D, and *BRAF* V600E geometric mean MFs for the DCs were 1.04×10^{-3}, 5.27×10^{-5}, 1.37×10^{-5}, 2.27×10^{-4}, and 6.49×10^{-6}, respectively (see Table 2). A comparison of the frequency distributions for *PIK3CA* H1047R, *KRAS* G12D, *KRAS* G12V, *HRAS* G12D, and *BRAF* V600E MFs in normal breast and DCs is shown in Figure 1. *HRAS* G12D MFs were significantly greater in DCs as compared to normal breast (two-tailed, Mann-Whitney rank sum test; P = .0033). No significant differences in MF were observed between normal breast and DCs for *PIK3CA* H1047R, *KRAS* G12D, *KRAS* G12V, or *BRAF* V600E.

Co-Occurrence of PIK3CA H1047R, KRAS G12D and G12V, HRAS G12D, and BRAF V600E Mutations in Normal Breast and DCs

The mean MF measurements for the five different hotspot point mutations *(PIK3CA* H1047R, *KRAS* G12D and G12V, *HRAS* G12D, and *BRAF* V600E) within individual samples are plotted in Figure 3*A* for normal breast and Figure 3*B* for DCs and the breast fat sample. All normal breast and DCs contained measureable levels of three or more cancer driver point mutations (at levels $\geq 10^{-5}$). For normal breast, 7/10 (70%) of samples had four mutations, and 3/10 (30%) of samples had three mutations at levels $\geq 10^{-5}$. For DCs, 6/9 (67%) of samples had four mutations, while 3/9 (33%) of samples had three mutations at levels $\geq 10^{-5}$. Table 3 describes the co-occurrence of hotspot point mutations in the DCs. For example, Table 3 shows that 9/9 (100%) of DCs carry *PIK3CA* H1047R, *KRAS* G12D, and *HRAS* G12D mutations.

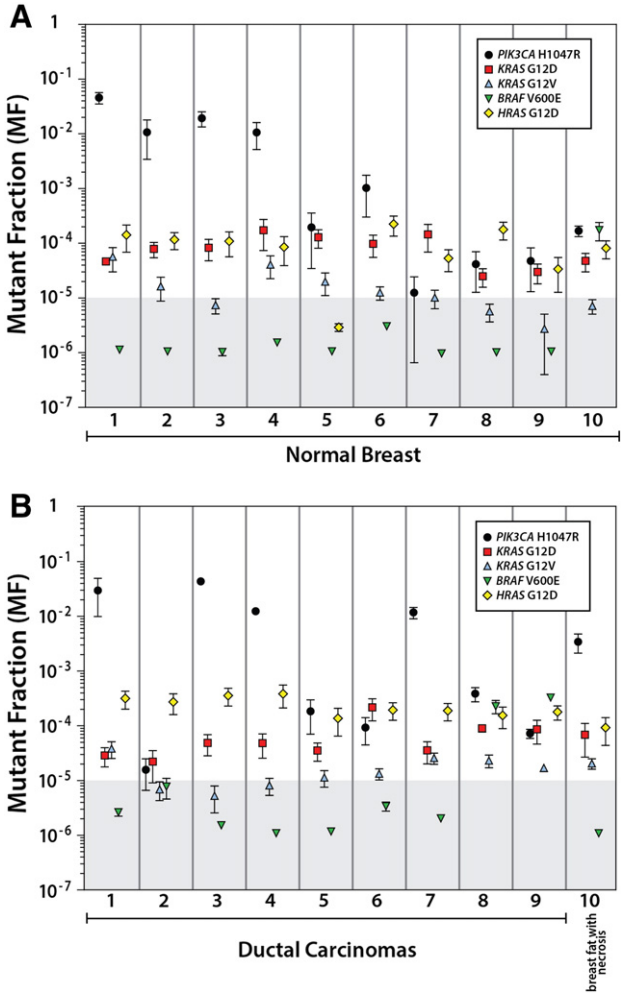

Figure 3. The co-occurrence of *PIK3CA* H1047R, *KRAS* G12D, *KRAS* G12V, *HRAS* G12D, and *BRAF* V600E mutation within individual samples. The average ACB-PCR MF measurements collected on ten normal breast samples are shown in (A). The average ACB-PCR MF measurements collected on nine DCs and one breast fat sample associated with a DC are shown in (B). Error bars denote the standard error of the mean. Measurements in the shaded areas ($<10^{-5}$) are below the limit of accurate ACB-PCR quantification.

Table 3. Co-occurrence of hotspot mutations in ductal carcinomas of the breast.

	PIK3CA H1047R	*KRAS* G12D	*KRAS* G12V	*HRAS* G12D	*BRAF* V600E
PIK3CA H1047R	-	100%	66.67%	100%	22.22%
KRAS G12D		-	66.67%	100%	22.22%
KRAS G12V			-	66.67%	22.22%
HRAS G12D				-	22.22%
BRAF V600E					-

PIK3CA H1047R MF Measurements in Normal Thyroid and PTCs

Our analyses identified 4/10 normal breast samples as having large subpopulations of *PIK3CA* H1047R mutant cells. However, we observed only a minor shift in the population distribution and geometric mean MF between normal breast and DCs (Figure 1). In order to clarify the significance of this result, we compared the ACB-PCR results obtained in breast, where the *PIK3CA* H1047R mutation is an established cancer driver mutation, to results obtained from thyroid, where there is no evidence that the *PIK3CA* H1047R mutation acts as a cancer driver mutation. Specifically, we measured *PIK3CA* H1047R MF in 20 normal thyroid and 20 PTCs, a cancer type with an exceedingly low reported frequency of *PIK3CA* H1047R mutation detection [2/1120; 0.18%]. The clinical and pathological information regarding the normal thyroid and PTC samples was reported previously [21]. The *PIK3CA* H1047R geometric mean MFs for normal thyroid and PTCs were 4.32×10^{-5} and 1.12×10^{-5}, respectively. For normal thyroid, 16/20 samples had detectable levels of the *PIK3CA* H1047R mutation. For PTCs, 7/20 samples had detectable levels of *PIK3CA* H1047R mutation. This is in contrast to breast, where all samples had measureable levels of the *PIK3CA* H1047R mutation. Furthermore, a significant decrease in *PIK3CA* H1047R mutation was observed in PTCs, as compared to normal thyroid (see Figure 4*A*). No significant correlation was observed between age and *PIK3CA* H1047R MF in normal thyroid (Pearson $r = 0.2898$, $P = .2762$; Figure 4*B*), unlike breast, where a significant positive correlation between age and *PIK3CA* H1047R MF was observed.

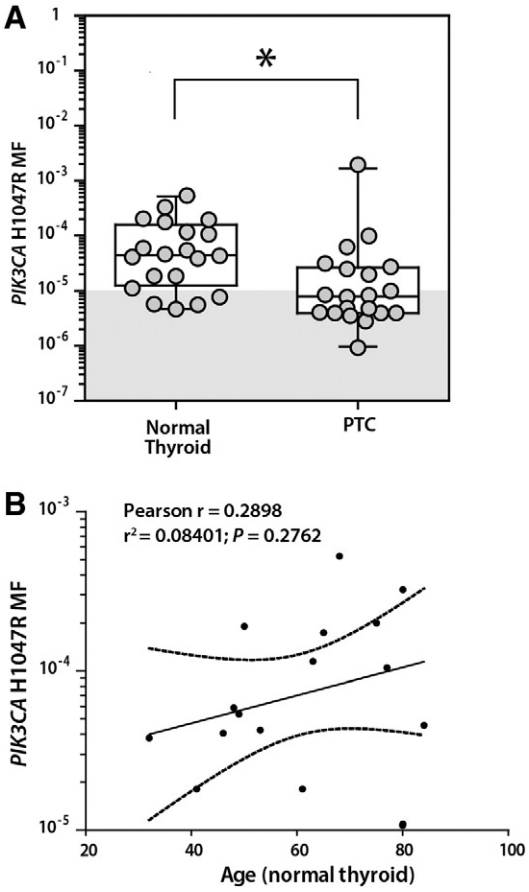

Figure 4. ACB-PCR analysis of normal thyroid tissue and papillary thryoid carcinomas. Individual measurements and box and whisker plots indicating the 5th, 25th, 50th, 75th, and 95th percentiles of the population distribution of *PIK3CA* H1047R MF measurements in normal thyroid and PTCs are presented in (A). Measurements in the shaded areas ($<10^{-5}$) are below the limit of accurate ACB-PCR quantification. The * indicates a significant difference in distribution of *PIK3CA* H1047R MFs greater than or less than 10^{-5} was observed between PTCs and normal thyroid samples (Fisher's exact test; $P = .0095$). Linear regression analysis depicts the relationship between normal thyroid tissue donor age and *PIK3CA* H1047R MF (B). MF measurements below the limit of accurate ACB-PCR quantification were not included in the linear regression analysis shown. No significant correlation with age was observed with or without including MFs $<10^{-5}$. Dashed lines describe the 95% confidence interval.

Discussion

The discovery that mutant cancer subpopulations limit patient responses to molecularly targeted, personalized cancer therapies has created an urgent public health need for knowledge regarding the prevalence and functional significance of such subpopulations (reviewed in [3,4]). To address this knowledge gap, and develop a new perspective on breast cancer heterogeneity, we performed sensitive and quantitative analyses of specific cancer driver mutations. This study focused on the measurement of the single most prevalent base substitution mutation reported in DCs (*PIK3CA* H1047R), two mutations rarely detected in DCs by DNA sequencing (*HRAS* G12D and *BRAF* V600E), and two mutations implicated in the development of acquired resistance to EGFR-targeted therapies (*KRAS* G12D and *KRAS* G12V). The mutant proteins encoded by these five activated oncogenes are attractive drug targets because of their prevalence across multiple cancer types. Knowledge regarding the fractions of cells carrying these mutations should inform the development of strategies to treat DCs.

The results of our DC analyses are qualitatively similar and consistent with published results, in that only the *PIK3CA* H1047R mutation was prevalent at levels detectable by DNA sequencing [7,10,26,27]. Beyond that, the results of this study extend current understanding of breast cancer heterogeneity in several ways. First, three of the five mutations analyzed were present at measureable levels in each DC analyzed, which is indicative of a remarkable level of tumor heterogeneity. Second, the *PIK3CA* mutation was present at some level in each of the DCs analyzed. And third, the low level of *HRAS* G12D mutation measured in DCs (geometric mean MF 2.27×10^{-4}) was significantly greater than that present in normal breast.

The therapeutic impact of *PIK3CA* mutation is an active area of investigation [18]. The prevalence of *PIK3CA* mutation in DCs is important because it has been reported to decrease time to progression in the context of trastuzumab treatment of HER2-

positive metastatic breast cancers [28]. A recent meta-analysis of breast cancer studies found that patients with *PIK3CA* mutant breast cancers had decreased relapse-free survival compared to patients with *PIK3CA* WT cancers, although this difference was seen only when trastuzumab was given in the neoadjuvant setting [29]. Recently, it has been suggested that *PIK3CA* mutations play different roles in early versus late ER-positive breast cancer [30]. In early breast cancer, *PIK3CA* mutation may be a marker of hormone dependence and good prognosis. In late/advanced breast cancers, it may contribute to anti-estrogen resistance. For such cancers, patients may benefit from combination treatment with an anti-estrogen and everolimus, an inhibitor of TORC1 (downstream in the PI3K/AKT pathway) [30].

Given the prevalence of the mutant *PIK3CA* in breast and other cancer types, targeting the mutant form of the protein is a viable therapeutic approach. Work is underway to characterize the protein binding pockets, in order to identify specific inhibitors of mutant *PIK3CA*, including the H1047R mutant protein [14,31]. Our observations indicate, however, that *PIK3CA* mutant DCs also carry *KRAS* G12D and *HRAS* G12D mutations, suggesting that ultimately there may be too many different subpopulations of driver mutations in advanced cancers to target individually.

This study employed the paradigm of comparing mutation levels in normal and cancer tissue, as a means of assessing the functional significance of the mutant subpopulations. This was based on the assumption that an increase in cancer MF (relative to normal) would indicate that the mutation provided a positive selective advantage during tumor progression. ACB-PCR has been used to show significant increases in *KRAS* G12D or *KRAS* G12V mutation in colon, lung, and thyroid tumors as compared to normal tissues [20–22]. However, no significant differences in *KRAS* G12D and *KRAS* G12V MF were observed between DCs and normal breast. Regarding *BRAF* V600E mutation, only two of nine DCs and one of ten normal breast samples had measureable levels of the mutation. A small, but significant increase in *HRAS* G12D mutation was detected in DC's compared to normal breast (2.27×10^{-4} versus 6.94×10^{-5}, respectively). These results suggest that the *HRAS* G12D mutation is playing a more significant role in breast cancer development than previously recognized. Of interest in this regard is a study by Cha *et al.*[32], which demonstrated that *N*-nitroso-*N*-methylurea-induced rat mammary tumors arose from spontaneous *Hras* G12D mutant cells of the mammary epithelium. The presence of *HRAS* and *KRAS* mutation, albeit at low frequencies, in human DCs should be considered carefully as investigators explore the potential use of EGFR inhibitors for the treatment of breast cancer [33,34].

The most striking observation of the current study was that all normal breast tissue samples had measureable levels of *PIK3CA* H1047R mutation, some at remarkably high levels. To our knowledge, there is only one previous report describing the detection of *PIK3CA* mutant cells in normal breast (samples that subsequent histopathological analysis identified as having columnar cell changes or metaplasia) [35]. The observation that the most prevalent point mutation identified in breast cancer is present at remarkably high levels in normal breast lends credence to the idea that mutant PI3K inhibitors might be used to prevent the development of breast cancer. But, assuming that levels of *PIK3CA* mutation in normal breast DNA could identify individuals at risk for developing breast cancer, it is unlikely that this could be used as a screening tool in healthy women. For this reason, there is considerable interest in analyzing liquid biopsies, even though the tissue origin of the marker(s) may not be readily known. For breast, however, DNA isolated from breast milk might be a viable, non-invasive approach for exploring the use of *PIK3CA* H1047R mutation as a quantitative biomarker of a woman's risk for developing breast cancer. This could be investigated first in women who have a family history of breast cancer, especially in families where the *PIK3CA* H1047R mutation was established as a driver of breast cancer.

We have been using ACB-PCR quantification as a means to investigate the tissue-specific "properties" of cancer driver mutations. For example, past analyses have identified both positive and negative selection of *KRAS* G12V mutation in colon and thyroid cancers. The positive selection was established by mutant enrichment in colonic adenomas or PTCs compared to normal [21,22]. The negative selection was established by an inverse correlation between MF and maximum tumor dimension for both tumor types, and a decrease in MF during adenoma to carcinoma progression for CRC [3,22]. The results of the current study allow us, for the first time, to characterize the selective advantage provided by a specific mutation in the context of normal breast. Specifically, linear regression analysis of *PIK3CA* H1047R MF in breast tissue from donors of different ages leads to the interpretation that the *PIK3CA* H1047R mutation increases as an exponential function in normal breast, with an ~ 10% increase in MF per year of age (Figure 2).

This study employed a comparison between breast and thyroid as evidence to support the hypothesis that subpopulations of *PIK3CA* H1047R mutation in normal breast drive the development of DC. Evidence suggests that the *PIK3CA* H1047R mutation is not a driver of papillary thyroid carcinogenesis. It is rarely detected in PTCs and there was no significant increase in MF with age for normal thyroid. While the *PIK3CA* H1047R mutation is present at relatively low levels in normal thyroid, it decreases significantly in PTCs. This is consistent with clonal expansion of non-PIK3CA mutant cells diluting out the low spontaneous level of PIK3CA mutant cells in thyroid. In contrast, remarkably high levels of *PIK3CA* H1047R are present in normal breast samples and these levels are maintained (as subpopulations) during progression to DCs. This supports the interpretation that the mutation provides a selective advantage to the developing tumor in the breast, but as a subpopulation.

A model depicting three possible pathways by which *PIK3CA* mutant subpopulations could contribute to the development of DCs is presented in Figure 5. Figure 5 is not intended to represent all possible mutations that can occur, nor capture the full extent of the co-occurrence of the multiple mutations that may exist as subpopulations. Figure 5, *A* and *B* depict the development of a *PIK3CA* H1047R mutant cancer from a single cell. According to Figure 5*A*, the DC develops from a *PIK3CA* mutant cell, in which case the mutation is present in all the malignant cells of the cancer. Presumably, this contributes to the fraction of *PIK3CA* mutant DCs that are detected by DNA sequencing. Figure 5*B* depicts the occurrence of *PIK3CA* mutation as a secondary event, thereby explaining its occurrence as a subpopulation. Figure 5*C* depicts tumor initiation as a polyclonal interaction between *PIK3CA* mutant and other mutant or epigenetically altered cells. Figure 5*C* incorporates the idea that *PIK3CA* mutant subpopulations provide a functional phenotype in trans that is necessary for the development of a predominant clone.

Several lines of evidence support the carcinogenic pathway depicted in Figure 5*C*. First, the frequency of *PIK3CA* mutation detection in DCs is lower than that detected in breast hyperplasia,

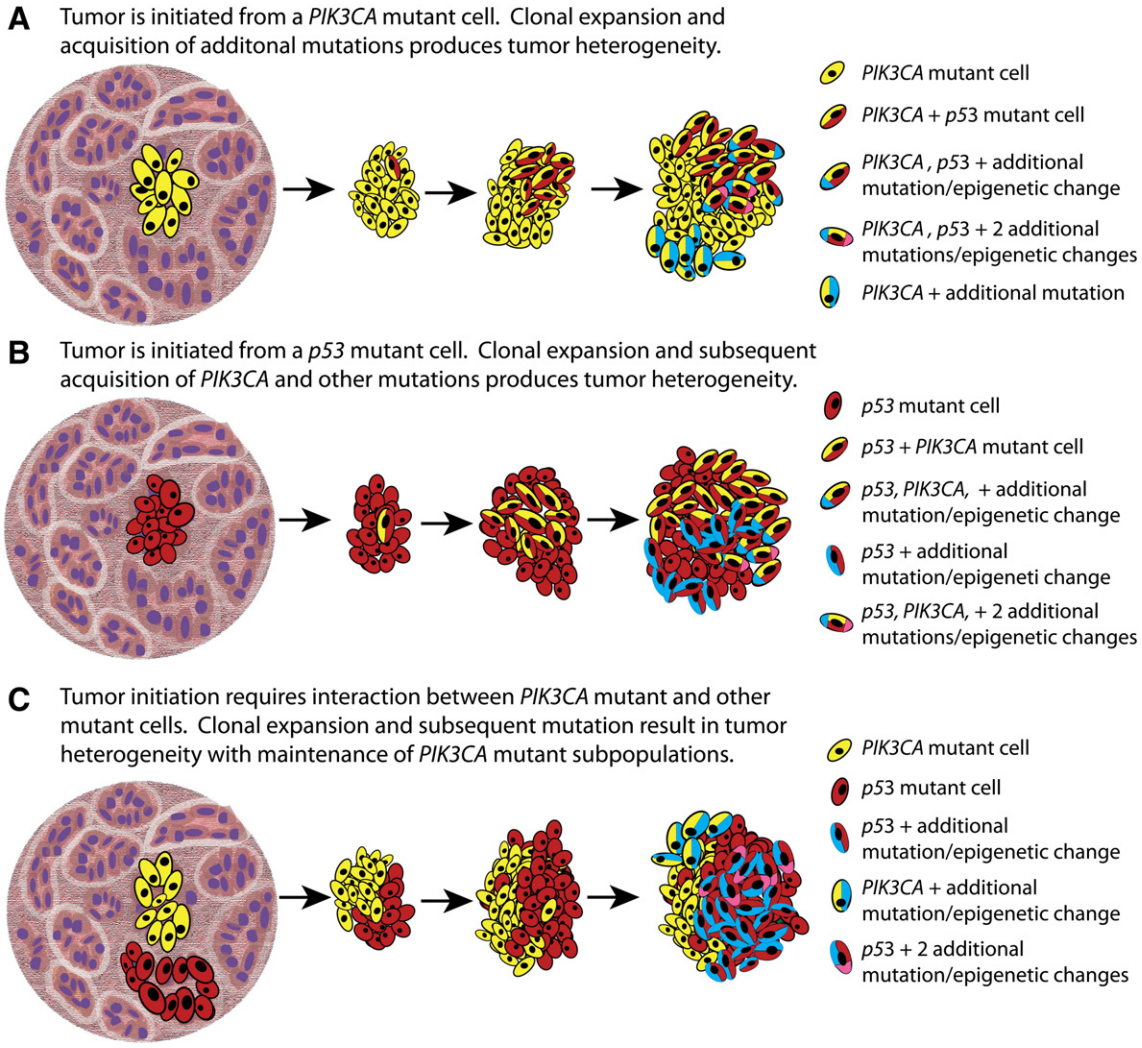

Figure 5. Alternate pathways to *PIK3CA*-induced DC. DCs could be initiated from a *PIK3CA* mutant cell, generating a cancer where the *PIK3CA* mutant cells predominate and the mutation would be detected by DNA sequencing (A). DCs could be initiated by a non-*PIK3CA* mutant cell, with *PIK3CA* mutation arising as a secondary event (B). DC could be initatiated through the interaction of *PIK3CA* and non-*PIK3CA* mutant clones with subsequent accumulation of mutation in both clonal populations (C). Pathways B and C have the potential to generate minor mutant subpopulations that could be detected by ACB-PCR, but not DNA sequencing.

according to data from the COSMIC database [7]. Ang *et al.*[27] found *PIK3CA* point mutations were detected in 31/62 (50%) of proliferative lesions (usual ductal hyperplasia and columnar cell change), with the *PIK3CA* H1047R mutation observed in 14/31 (45%) of the usual ductal hyperplasia samples. The same study found *PIK3CA* H1047R mutation in 13/37 (35%) of invasive carcinomas [27]. This is consistent with Figure 5*C*, which depicts *PIK3CA* H1047R as a marker of susceptibility and an early driver of DC, which may be outgrown by other transformed clones in the fully developed cancer. Conversely, the more frequent detection of *PIK3CA* mutation in hyperplasia than in DC cannot be explained easily by the pathways depicted in Figure 5*A* or *B*, unless one assumes *PIK3CA* mutant breast hyperplasia does not contribute to DC.

Several studies provide direct evidence of clonal cooperation driving the development of tumor heterogeneity in mammalian systems. Using a xenograft model to reproduce a frequent pattern of EGFR heterogeneity in human glioblastomas, Inda et al. [36] demonstrated that that a minor, EGFR mutant subclone could drive the growth of a predominant, EGFR WT clone via a cytokine-mediated mechanism. Subsequently, Marusyk *et al.*[37] demonstrated that cooperation between populations of clones (constructed by lentivirus infection of a breast cancer cell line) can generate a tumor-promoting microenvironment that stimulates tumor growth, with driver subclones retained as minor subpopulations. By investigating how a subpopulation of cells carrying an *Hras* oncogene behaves when present with the parental cells (recapitulates a monoclonal tumor origin) versus when present with other mutant subclones, Cleary *et al.*[38] provided evidence of inter-clonal cooperation between the WNT1 producing luminal cells and mutant *Hras* expressing basal cells. Further support for the idea that activated oncogenes drive tumor progression "in trans" via a secretory mechanism comes from a study by Hobor *et al.*[39]. They showed that colorectal cells sensitive to EGFR blockade can grow in the presence of cetuximab when co-cultured with resistant cells or with conditioned media from resistant cells, due to a mechanism involving secretion of TGFα and amphiregulin. Therefore, some

activated oncogenes frequently found as cancer subpopulations may have capabilities as "transdriver mutations," meaning they drive progression of a predominant clone through paracrine mechanisms. Intratumoral heterogeneity and cooperativity between tumor subpopulations has been demonstrated in a Trp53-null mouse model of human breast cancer [40].

Some investigators have reached the conclusion that breast cancers can be polyclonal in origin [41]. However, the "lasting paradigm" that cancer is a disease of clonal growth that develops from a normal precursor cell is a concept still held strongly by many [42]. In fact, a recent cancer textbook concludes that there "is a widespread consensus that the vast majority of advanced human tumors are monoclonal growths descended from single normal progenitor cells that took the first small steps to becoming cancerous" [43]. However, adherence to the theory of monoclonal tumor origin has been questioned [44]. This controversy is clearly related to the technical difficulty associated with assessing the earliest events in carcinogenesis. Nevertheless, quantification of cancer driver mutations in normal breast and DCs supports the interpretation that *PIK3CA* H1047R mutation is a major driver of polyclonal DC initiation. Observations from the literature, in conjunction with the data reported here, suggest that: 1) spontaneous cancer driver mutations are not rare, 2) cancer initiation often involves cooperative clonal interactions, and 3) mutations that frequently appear as cancer subpopulations may represent a class of "transdriver oncogenes."

Conclusions

Hotspot cancer driver mutations *PIK3CA* H1047R, *KRAS* G12D, *HRAS* G12D, and to a lesser extent *KRAS* G12V are present in normal breast tissue. The *PIK3CA* H1047R mutation is present at remarkably high levels in some normal breast tissue samples and the levels of this mutation increase with age. This suggests *PIK3CA* H1047R mutation may be a biomarker of breast cancer susceptibility and could be a therapeutic target for breast cancer prevention. Subpopulations of *PIK3CA* H1047R, *KRAS* G12D, *KRAS* G12V, and *HRAS* G12D are prevalent in DCs, with 9/9 (100%) of DCs carrying at least three of these mutations. Only the *HRAS* G12D mutation, however, was present at a significantly greater level in DC than in normal breast. This study illustrates how high-sensitivity quantification of cancer driver mutations can complement data from large-scale cancer genome sequencing to elucidate the role of cancer driver mutations in carcinogenesis and to guide strategies for therapeutic intervention.

Acknowledgements

The authors thank Dr. Igor Pogribny, Dr. Vasily Dobrovolsky, and Dr. Robert H. Heflich for their helpful review of the manuscript and thank Melanie Raymundo and Larry Pastor for their assistance with the QClamp analysis. Tissue samples were provided by the Cooperative Human Tissue Network which is funded by the National Cancer Institute. Other investigators may have received specimens from the same subjects. This study was supported by the National Center for Toxicological Research and the U.S. Food and Drug Administration. The information in these materials is not a formal dissemination of information by FDA and does not represent agency position or policy.

Appendix A. Supplementary Data

Supplementary data to this article can be found online at http://dx.doi.org/10.1016/j.neo.2016.03.002.

References

[1] Parsons BL and Meng F (2009). K-RAS mutation in the screening, prognosis and treatment of cancer. *Biomark Med* **3**, 757–769.
[2] Oikonomou E, Koustas E, Goulielmaki M, and Pintzas A (2014). BRAF vs RAS oncogenes: Are mutations of the same pathway equal? Differential signalling and therapeutic implications. *Oncotarget* **5**, 11752–11777.
[3] Parsons BL and Myers MB (2013). KRAS mutant tumor subpopulations can subvert durable responses to personalized cancer treatments. *Pers Med* **10**, 191–199.
[4] Parsons BL and Myers MB (2013). Personalized cancer treatment and the myth of KRAS wild-type colon tumors. *Discov Med* **15**, 259–267.
[5] Diaz Jr LA, Williams RT, Wu J, Kinde I, Hecht JR, Berlin J, Allen B, Bozic I, Reiter JG, and Nowak MA, et al (2012). The molecular evolution of acquired resistance to targeted EGFR blockade in colorectal cancers. *Nature* **486**, 537–540.
[6] Misale S, Yaeger R, Hobor S, Scala E, Janakiraman M, Liska D, Valtorta E, Schiavo R, Buscarino M, and Siravegna G, et al (2012). Emergence of KRAS mutations and acquired resistance to anti-EGFR therapy in colorectal cancer. *Nature* **486**, 532–536.
[7] Catalogue of Somatic Mutations in Cancer. http://cancer.sanger.ac.uk/cancergenome/projects/cosmic/; 2015.
[8] The Cancer Genome Atlas Research Network (2013). The Cancer Genome Atlas Pan-Cancer analysis project. *Nat Genet* **45**, 1113–1120. http://dx.doi.org/10.1038/ng.2764.
[9] cBioPortal for Cancer Genomics. http://www.cbioportal.org/public-portal/.
[10] Wang Y, Waters J, Leung ML, Unruh A, Roh W, Shi X, Chen K, Scheet P, Vattathil S, and Liang H, et al (2014). Clonal evolution in breast cancer revealed by single nucleus genome sequencing. *Nature* **512**, 155–160.
[11] Schmitt MW, Fox EJ, Prindle MJ, Reid-Bayliss KS, True LD, Radich JP, and Loeb LA (2015). Sequencing small genomic targets with high efficiency and extreme accuracy. *Nat Methods* **12**, 423–425.
[12] Myers MB, Wang Y, McKim KL, and Parsons BL (2012). Hotspot oncomutations: Implications for personalized cancer treatment. *Expert Rev Mol Diagn* **12**, 603–620.
[13] The Cancer Genome Atlas. http://cancergenome.nih.gov/.
[14] Gkeka P, Evangelidis T, Pavlaki M, Lazani V, Christoforidis S, Agianian B, and Cournia Z (2014). Investigating the Structure and Dynamics of the PIK3CA Wild-Type and H1047R Oncogenic Mutant. *PLoS Comput Biol* **10**.
[15] Kang S, Bader AG, and Vogt PK (2005). Phosphatidylinositol 3-kinase mutations identified in human cancer are oncogenic. *Proc Natl Acad Sci U S A* **102**, 802–807.
[16] Janku F, Wheler JJ, Naing A, Falchook GS, Hong DS, Stepanek VM, Fu S, Piha-Paul SA, Lee JJ, and Luthra R, et al (2013). PIK3CA mutation H1047R is associated with response to PI3K/AKT/mTOR signaling pathway inhibitors in early-phase clinical trials. *Cancer Res* **73**, 276–284.
[17] Hart JR, Zhang Y, Liao L, Ueno L, Du L, Jonkers M, Yates JR, and Vogt PK (2015). The butterfly effect in cancer: A single base mutation can remodel the cell. *Proc Natl Acad Sci U S A* **112**, 1131–1136.
[18] Dieci MV and Guarneri V (2015). PIK3CA: a Target or a Marker in Breast Cancers. *Curr Breast Cancer Rep* **7**, 161–169.
[19] De Roock W, Claes B, Bernasconi D, De Schutter J, Biesmans B, Fountzilas G, Kalogeras KT, Kotoula V, Papamichael D, and Laurent-Puig P, et al (2010). Effects of KRAS, BRAF, NRAS, and PIK3CA mutations on the efficacy of cetuximab plus chemotherapy in chemotherapy-refractory metastatic colorectal cancer: A retrospective consortium analysis. *Lancet Oncol* **11**, 753–762.
[20] Myers MB, McKim KL, Meng F, and Parsons BL (2015). Low-frequency KRAS mutations are prevalent in lung adenocarcinomas. *Pers Med* **12**, 83–98.
[21] Myers MB, McKim KL, and Parsons BL (2014). A subset of papillary thyroid carcinomas contain KRAS mutant subpopulations at levels above normal thyroid. *Mol Carcinog* **53**, 159–167.
[22] Parsons BL, Marchant-Miros KE, Delongchamp RR, Verkler TL, Patterson TA, McKinzie PB, and Kim LT (2010). ACB-PCR quantification of K-RAS codon 12 GAT and GTT mutant fraction in colon tumor and non-tumor tissue. *Cancer Investig* **28**, 364–375.
[23] Prior IA, Lewis PD, and Mattos C (2012). A comprehensive survey of ras mutations in cancer. *Cancer Res* **72**, 2457–2467.
[24] Hollestelle A, Elstrodt F, Nagel JHA, Kallemeijn WW, and Schutte M (2007). Phosphatidylinositol-3-OH kinase or RAS pathway mutations in human breast cancer cell lines. *Mol Cancer Res* **5**, 195–201.
[25] Michael M, Ganta M, Peletskaya E, Pastor L, Raymundo M, Wu G, Wang J, and Zhang A (2015). High Sensitivity Detection of Tumor Gene Mutations. *BAOJ Cancer Res Ther* **1**, 1–6.

[26] Koboldt DC, Fulton RS, McLellan MD, Schmidt H, Kalicki-Veizer J, McMichael JF, Fulton LL, Dooling DJ, Ding L, and Mardis ER, et al (2012). Comprehensive molecular portraits of human breast tumours. *Nature* **490**, 61–70.

[27] Ang DC, Warrick AL, Shilling A, Beadling C, Corless CL, and Troxell ML (2014). Frequent phosphatidylinositol-3-kinase mutations in proliferative breast lesions. *Mod Pathol* **27**, 740–750.

[28] Razis E, Bobos M, Kotoula V, Eleftheraki AG, Kalofonos HP, Pavlakis K, Papakostas P, Aravantinos G, Rigakos G, and Efstratiou I, et al (2011). Evaluation of the association of PIK3CA mutations and PTEN loss with efficacy of trastuzumab therapy in metastatic breast cancer. *Breast Cancer Res Treat* **128**, 447–456.

[29] Ibrahim EM, Kazkaz GA, Al-Mansour MM, and Al-Foheidi ME (2015). The predictive and prognostic role of phosphatase phosphoinositol-3 (PI3) kinase (PIK3CA) mutation in HER2-positive breast cancer receiving HER2-targeted therapy: a meta-analysis. *Breast Cancer Res Treat* **152**, 463–476.

[30] Mayer IA and Arteaga CL (2014). PIK3CA activating mutations: A discordant role in early versus advanced hormone-dependent estrogen receptor-positive breast cancer? *J Clin Oncol* **32**, 2932–2934.

[31] Massacesi C, Di Tomaso E, Fretault N, and Hirawat S (2013). Challenges in the clinical development of PI3K inhibitors; 2013 19–23.

[32] Cha RS, Thilly WG, and Zarbl H (1994). N-nitroso-N-methylurea-induced rat mammary tumors arise from cells with preexisting oncogenic Hras1 gene mutations. *Proc Natl Acad Sci U S A* **91**, 3749–3753.

[33] Jamdade VS, Sethi N, Mundhe NA, Kumar P, Lahkar M, and Sinha N (2015). Therapeutic targets of triple-negative breast cancer: A review. *Br J Pharmacol* **172**, 4228–4237.

[34] Yewale C, Baradia D, Vhora I, Patil S, and Misra A (2013). Epidermal growth factor receptor targeting in cancer: A review of trends and strategies. *Biomaterials* **34**, 8690–8707.

[35] Ang D, O'Gara R, Schilling A, Beadling C, Warrick A, Troxell ML, and Corless CL (2013). Novel method for PIK3CA mutation analysis: Locked nucleic acid-PCR sequencing. *J Mol Diagn* **15**, 312–318.

[36] Inda MDM, Bonavia R, Mukasa A, Narita Y, Sah DWY, Vandenberg S, Brennan C, Johns TG, Bachoo R, and Hadwiger P, et al (2010). Tumor heterogeneity is an active process maintained by a mutant EGFR-induced cytokine circuit in glioblastoma. *Genes Dev* **24**, 1731–1745.

[37] Marusyk A, Tabassum DP, Altrock PM, Almendro V, Michor F, and Polyak K (2014). Non-cell-autonomous driving of tumour growth supports sub-clonal heterogeneity. *Nature* **514**, 54–58.

[38] Cleary AS, Leonard TL, Gestl SA, and Gunther EJ (2014). Tumour cell heterogeneitymaintained by cooperating subclones in Wnt-driven mammary cancers. *Nature* **509**, 113–117.

[39] Hobor S, Van Emburgh BO, Crowley E, Misale S, Di Nicolantonio F, and Bardelli A (2014). TGFα and amphiregulin paracrine network promotes resistance to EGFR blockade in colorectal cancer cells. *Clin Cancer Res* **20**, 6429–6438.

[40] Zhang M, Tsimelzon A, Chang C-H, Fan C, Wolff A, Perou CM, Hilsenbeck SG, and Rosen JM (2015). Intratumoral Heterogeneity in a Trp53-Null Mouse Model of Human Breast Cancer. *Cancer Discov* **5**, 520–533.

[41] Going JJ (2003). Epithelial carcinogenesis: Challenging monoclonality. *J Pathol* **200**, 1–3.

[42] Rivenbark AG and Coleman WB (2012). Field cancerization in mammary carcinogenesis - Implications for prevention and treatment of breast cancer. *Exp Mol Pathol* **93**, 391–398.

[43] Weinberg RA (2013). The Biology of Cancer. Garland Scientific, New York, New York; 2013. p. 3–69.

[44] Parsons BL (2008). Many different tumor types have polyclonal tumor origin: Evidence and implications, Mutation Research. *Rev Mutat Res* **659**, 232–247.